Published in final edited form as:
Magn Reson Med. 2014 September ; 72(3): 829–840. doi:10.1002/mrm.24956.

Imaging neurodegeneration in the mouse hippocampus after neonatal hypoxia-ischemia using oscillating gradient diffusion MRI

Manisha Aggarwal[1], **Jennifer Burnsed**[2], **Lee J. Martin**[3,4], **Frances J. Northington**[2], and **Jiangyang Zhang**[1]

[1]Russell H. Morgan Department of Radiology and Radiological Science, Johns Hopkins University School of Medicine, Baltimore, Maryland, USA

[2]Department of Pediatrics, Johns Hopkins University School of Medicine, Baltimore, Maryland, USA

[3]Department of Neuroscience, Johns Hopkins University School of Medicine, Baltimore, Maryland, USA

[4]Division of Neuropathology, Johns Hopkins University School of Medicine, Baltimore, Maryland, USA

Abstract

Purpose—To investigate if frequency-dependent contrasts using oscillating gradient diffusion MRI (dMRI) can detect hypoxia-ischemia (HI) induced neurodegeneration in the neonatal mouse hippocampus.

Methods—Pulsed- and oscillating-gradient dMR images (at 50, 100, and 150 Hz) were acquired from postmortem fixed brains of mice exposed to neonatal HI using the Rice-Vanucci model. MRI data were acquired at 1, 4, and 8 days following HI, and compared with histological data from the same mice for *in situ* histological validation of the MRI findings.

Results—The rate of change of apparent diffusion coefficient with gradient frequency (Δ_fADC) revealed unique layer-specific contrasts in the neonatal mouse hippocampus. Δ_fADC measurements were found to show a significant decrease in response to neonatal HI injury, in the pyramidal (Py) and granule (GrDG) cell layers compared to contralateral regions. The areas of reduced intensity in the Δ_fADC maps corresponded to regional neurodegeneration seen with H&E and Fluoro-Jade C stainings, indicating that alterations in Δ_fADC contrasts are sensitive to early microstructural changes due to HI-induced neurodegeneration in the studied regions.

Conclusion—The findings show that the frequency-dependence of ADC measurements with oscillating-gradient dMRI can provide a sensitive contrast to detect HI-induced neurodegeneration in neuronal layers of the neonatal mouse hippocampus.

Correspondence to: Jiangyang Zhang, Ph.D., Traylor Building, Room#208, Johns Hopkins University School of Medicine, 720 Rutland Avenue, Baltimore, MD 21205, USA, jzhang3@jhmi.edu, Phone: (410) 502-9856, Fax: (410) 614-1948.

Keywords

diffusion MRI; oscillating gradient; hypoxia-ischemia; neonatal; mouse hippocampus

INTRODUCTION

Neonatal hypoxia-ischemia (HI) is associated with significant damage to both grey and white matter, and can lead to severe long-term neurological sequelae [1]. To study the mechanisms and outcomes of HI-related brain injury, rodent models of neonatal HI have been established and are widely used [2, 3]. Studies in these models have shown that HI induces significant neuronal injury in selectively vulnerable brain regions, including the hippocampus, basal ganglia, and cerebral cortex, and the neurodegeneration in these regions evolves progressively after the initial injury [4–6]. HI-induced neurodegeneration in the immature hippocampus has been the focus of several studies in HI rodent models, both because of the selective vulnerability of the hippocampus to HI and its potential regenerative capacity. Findings based on histopathological assessment have shown that the pyramidal cells in the CA1–CA3 regions of the hippocampus, and the granule cells in the dentate gyrus undergo selective neurodegeneration following HI [7–11].

Magnetic resonance imaging (MRI) provides several diagnostic markers for the detection of neonatal HI-induced injury, and has been used clinically to establish the pattern of injuries and predict neurologic outcomes in term infants with HI [12]. MRI has also been used to monitor the neuropathology in rodent models of HI. Conventional diffusion MRI (dMRI) and T_2-weighted MRI are sensitive to acute cytotoxic edema and subsequent vasogenic edema following HI, respectively, and have been used in studies of HI models [13–15], while diffusion tensor imaging has been used to assess the progression of white matter injury [16, 17]. Measurements of the apparent diffusion coefficient (ADC) with dMRI have been routinely used to evaluate brain injury following HI in the rodent brain [13, 14]. A few recent studies using dMRI in rodent models have shown that changes in diffusivity measurements in the hippocampus correlate with neuronal injury and glial activation following HI [18, 19]. However, detailed examination of hippocampal neurodegeneration induced by HI has mostly relied on post-mortem neurohistology, due to a lack of specific MR contrasts that can delineate neuronal damage in the hippocampus.

Recently, dMRI using oscillating-gradient waveforms was shown to enable the acquisition of diffusion measurements in the ultra-short diffusion time regime (e.g., 5 ms or less) [20, 21]. With effective diffusion times much shorter than those typically achievable with conventional pulsed-gradient dMRI, oscillating-gradient dMRI can potentially provide more specific information on local tissue microenvironment [22, 23]. Several studies have demonstrated that oscillating gradient dMRI measurements obtained over a range of gradient frequencies can reveal information on the relative spatial scales of microscopic barriers restricting diffusion, in phantoms [24–26] and in rodent brains in vivo [27–29] and ex vivo [29–31]. Further, the differential dependence of ADC measurements on gradient frequency in different regions of the fixed rodent brain was recently shown to generate novel tissue contrasts in grey matter regions, especially the pyramidal and the granule cell layers in the

adult rodent hippocampus [30, 31], regions that are selectively vulnerable to HI injury. It was also shown that the frequency dependence of ADC contrasts corresponded closely with the intensity of nuclei-specific histological staining in the mouse brain, suggesting that the observed contrasts were associated with underlying cytoarchitectural features such as cell density in these regions [31]. Because the rates of water diffusion in brain tissue are determined by the cellular and molecular tissue composition, they are directly influenced by changes in tissue microstructure associated with neuropathological events, such as neurodegeneration and reactive glial and vascular changes. Therefore, we hypothesized that the frequency-dependent ADC contrasts observed with oscillating gradient dMRI can be sensitive to early microstructural changes associated with HI-induced neurodegeneration in the hippocampal neuronal layers.

In this study, we used the well-established Rice-Vanucci mouse model of neonatal HI [32] to test the hypothesis. The neuropathology in this model has been previously well-studied using histological staining techniques. Oscillating-gradient diffusion MR images with different gradient frequencies were acquired from post-mortem fixed brains of mice that were exposed to neonatal HI. To investigate if changes in the frequency-dependent ADC contrasts can detect the early temporal evolution of injury after HI in the neonatal brain, MRI data were acquired from mice sacrificed at three time points (1, 4, and 8 days) after exposure to neonatal HI, and later compared to histological data from the same animals in order to characterize the underlying histopathological correlates of the MRI findings.

METHODS

Animals and neonatal hypoxia-ischemia

Postnatal day 7 (P7) C57BL6 mouse pups were subjected to HI using the Vanucci model adapted for neonatal mice as described previously (unilateral ligation of the right carotid artery followed by 45 minutes of hypoxia, FiO_2=0.08) [32, 33]. Mice were sacrificed at 1, 4, and 8 days after HI (P8, P11 and P15, n=5 at each age) and transcardially perfused with 4% paraformaldehyde (PFA) in phosphate buffered saline (PBS) for ex vivo MRI and histology. Three mice were subjected only to unilateral carotid artery ligation without hypoxia (sham-injured), and sacrificed at P8. At each time point, age-matched naïve mice (n=5 each at P8, P11, and P15) were used as controls. After fixation, the mouse heads were removed and immersed in 4% PFA in PBS for 24 hours, and then transferred to PBS with 2 mM gadopentetate dimeglumine (Magnevist, Berlex Imaging, Wayne, NJ, USA) for 48 hours. For MRI, the specimens were placed in custom-built glass tubes that were filled with fomblin (Fomblin Perfluoropolyether, Solvay Solexis, Thorofare, NJ, USA) for susceptibility matching and to prevent dehydration. All animal procedures were approved by the Animal Use and Care Committee at the Johns Hopkins University School of Medicine.

MR image acquisition

MR imaging of the mouse heads was performed on a vertical-bore 11.7-Tesla NMR spectrometer (Bruker Biospin, Billerica, MA, USA) equipped with a Micro2.5 gradient system (maximum gradient strength of 1000 mT/m), using a 15-mm diameter volume coil for radiofrequency transmission/reception. The temperature of the specimens was

maintained at 37°C during imaging via the spectrometer's temperature control system. Conventional pulsed-gradient diffusion MR images were first acquired for diffusion tensor mapping, using a diffusion-weighted gradient and spin echo (DW-GRASE) sequence with navigator echo phase correction [34], with a rare-factor of 4, three echoes per refocusing pulse, echo time (TE)/repetition time (TR) of 33/800 ms, four signal averages, and diffusion gradient duration (δ)/separation (Δ) = 3.2/15 ms. Two images with minimal diffusion weighting (b_0 images) and nine images with relatively heavy diffusion weighting (b-value ~1200 s/mm^2) were acquired, at an isotropic native spatial resolution of 100 × 100 × 100 μm^3. The field-of-view (FOV) and matrix size ranged from 12.0 × 9.6 × 14.4 mm^3 to 12.8 × 10.0 × 15.6 mm^3 and 120 × 96 × 144 to 128 × 100 × 156 for the P8 to P15 specimens, respectively. Three sets of co-registered 3D diffusion-weighted images were then acquired with the same resolution and fields-of-view as the pulsed-gradient data, using a DW-GRASE sequence that was modified with cosine-modulated oscillating diffusion-sensitizing gradient waveforms as previously described in Parsons *et al*. [26]. The sequence parameters for acquisition were identical to those used for the pulsed-gradient DW-GRASE sequence, with TE/TR = 50/800 ms, and the duration of the diffusion-sensitizing gradients equal to 20 ms. Data were acquired at three different gradient oscillation frequencies of 50, 100, and 150 Hz (effective diffusion times of 5, 2.5, and 1.67 ms, respectively, computed according to Ref. [26]). At each frequency, one b_0 image and diffusion-weighted images (b-value ~700 s/mm^2) in four tetrahedral diffusion directions: [1,1,1], [−1,1,1], [1,−1,1], and [1,1,−1] were acquired for ADC mapping. The b-value for oscillating-gradient experiments was kept constant at 700 s/mm^2, as this was the maximum attainable value within gradient hardware limits for the diffusion-encoding gradients at 150 Hz. The total acquisition time ranged from 25 to 31.5 hours for the P8 to P15 mouse heads.

Data analysis

The *k*-space data were apodized by a symmetric trapezoidal function with 10% ramp widths to reduce noise, and zero-filled to twice the native matrix size prior to Fourier transformation. Diffusion tensor fitting for the pulsed-gradient dMRI data was performed using a log-linear fitting method, and maps of fractional anisotropy (FA) were calculated from the fitted tensor data. Isotropic diffusion weighted (iDW) images were generated by taking the mean intensity at each voxel of diffusion-weighted images along isotropically-distributed diffusion directions. ADC maps at each gradient frequency were calculated by averaging the diffusion coefficients computed along each of the four tetrahedral directions by $D^{(k)} = -\ln\left(\frac{S^{(k)}}{S_o}\right)/b$, where $S^{(k)}$ is the signal intensity for the *k*-th direction and S_0 is the intensity of the b_0 image [35]. To compute the frequency-dependence of ADC measurements in the brain, a linear least squares fitting of ADC with the gradient oscillation frequency was performed using IDL (ITT Visual Information Solutions, Boulder, AZ). The resulting maps (referred to as Δ_fADC here) represent the rate of change in ADC with the frequency of the oscillating gradients. The ADC measurements were fit to a linear model, since the frequency-dependence of ADC within the relatively narrow frequency range used in this study can be closely approximated by a linear curve as shown previously [31].

For analysis, the signals from the skull were manually removed in the iDW images, using Amira (Mercury Computer Systems, Inc., USA). The skull-stripped images of each mouse were first aligned to age-matched mouse brain MRI atlases [36], using intensity-based linear rigid registration [37]. The aligned images were then warped to the age-matched atlas at each age (P8, P11, and P15), using two-channel large deformation diffeomorphic metric mapping (LDDMM) based on iDW and FA contrasts [38]. The LDDMM procedure was driven by iDW and FA contrasts in order to ensure accurate alignment of both the overall brain morphology and internal structures within the brain, respectively (Fig. 1). The derived diffeomorphic transformations were then applied to the iDW images, ADC maps at each frequency, and the Δ_fADC maps, from which group-averaged iDW, ADC, and Δ_fADC images were generated for the HI-injured and control groups at each time point.

For measurements of ADC and Δ_fADC, regions of interest (ROIs) were manually segmented in the pyramidal cell layer (Py) in the CA1 hippocampal subfield and the granular cell layer in the dentate gyrus (GrDG) at the level of the dorsal hippocampus in the group-averaged maps, using ROIEditor (www.mristudio.org). Bilateral ROIs were segmented on four coronal slices in the left and right hippocampi at each age, for each of the GrDG and Py layers. The mean ADC measurements at each frequency and the mean Δ_fADC value in the ROIs were obtained for all individual mice. Student's two-tailed t-tests were used for group comparison and comparison between ipsilateral and contralateral measurements. Statistical analysis was performed using MATLAB (MathWorks, Natick, MA, USA).

Tissue processing and histopathology

The same mice used for MR imaging were also used for histology studies. After imaging, brains were removed from skulls and soaked in paraformaldehyde for 48 hours prior to processing. Specimens were processed at the Tissue Microarray Laboratory at Johns Hopkins Medical Institute in Baltimore, Maryland. The brains were processed in an automated tissue processor (Tissue-Tek VIP 2000, Sakura Finetek, Torrance, CA) for paraffin embedding of tissue. The paraffin embedded brains were then sectioned into coronal slices of 5 microns thickness, and mounted on slides coated with poly-L-lysine. The slides were dried overnight and then baked in a dry oven at 60°C prior to staining. Select slides were stained with hematoxylin and eosin (H&E) using a Leica AutoStainer XL (Leica Biosystems, Richmond, Virginia, USA). H&E staining was used to assess neuronal injury following HI because both apoptotic and necrotic neurons, and their structural variants, can be identified on H&E-stained sections by their morphological features [6]. Staining of the mounted slides with Fluoro-jade C (Chemicon, Temecula, CA) was performed using previously described methods [39], for detection of neuronal degeneration. Fluoro-jade C has been shown to stain degenerating neurons regardless of specific insult or mechanism of cell death, with a high signal to background ratio [39]. Histological images were obtained at a magnification of 10x and 40x using light microscopy.

RESULTS

Delineation of Py and GrDG layers in the neonatal mouse hippocampus

ADC measurements with oscillating-gradient dMRI at increasing gradient frequencies revealed strong contrast enhancement in specific regions in the neonatal mouse brain, which appeared relatively homogeneous in the pulsed-gradient ADC maps (Fig. 2). An increase in ADC values with gradient frequency was observed in most regions of the neonatal brain, and the frequency-dependent increase was significantly higher in specific neuronal layers in the hippocampus, the cerebellum, and the olfactory bulb, compared to other brain regions. In the neonatal hippocampus, the significant increase in ADC with gradient frequency was found to be specific to both the Py ($p < 0.005$) and the GrDG ($p < 0.005$) layers, whereas neighboring hippocampal regions showed only moderate frequency-dependent increase in ADC. The plot in Fig. 2 compares the ADC measurements from the hippocampal Py and GrDG layers and an adjacent region in the CA1 subfield from control mice at P8 (mean ± standard deviation, n=5). While ADC values in these three regions did not differ significantly in the zero frequency range (measured using the pulsed-gradient sequence), a significant ($p < 0.005$) progressive increase in the differences between ADC values of the Py and GrDG layers and ADC values of adjacent hippocampal regions was observed with increasing gradient frequencies. Maps of Δ_fADC derived from a linear fitting of the ADC measurements with gradient frequency show the frequency-dependent anatomical contrasts observed in the P8 mouse brain, with prominent delineation of the Py and GrDG layers in the hippocampus (Fig. 2).

HI-induced hippocampal neurodegeneration detected with oscillating gradient dMRI

At twenty-four hours after neonatal HI injury (at P8), a marked decrease in the Δ_fADC values was detected in the Py layer of the ipsilateral CA1 hippocampal region (1.52 ± 0.34 μm^2) compared to the contralateral side (2.05 ± 0.23 μm^2) (Fig. 3a). H&E staining revealed pockets of apparent cell loss with pyknotic nuclei and decreased neuronal density in the Py layer of the ipsilateral CA1 subfield, which corresponded to regions of decreased intensity observed in the Δ_fADC maps (Fig. 3b–c, f–g). The H&E-stained sections showed no apparent neuronal loss in the caudal CA2 and CA3 regions (Fig. 3c), and the corresponding regions in the Δ_fADC map also showed relatively unchanged values (Fig. 3a). Fluoro-jade C staining, a marker of neurodegeneration and reactive gliosis, showed evidence of degenerative changes in the ipsilateral CA1 region at this stage (Fig. 3e, i). In contrast, the contralateral hippocampus exhibited no apparent injury on the H&E and Fluoro-Jade C stained sections (Fig. 3d, h) and in the Δ_fADC maps. No significant differences in measured Δ_fADC values were found between the ipsilateral and contralateral dentate gyrus. Histological evaluation showed no apparent injury in the GrDG region in the H&E stained sections (Fig. 3c), while Fluoro-Jade C staining revealed scattered degenerative changes in the dentate gyrus at 24 hours after the injury (Fig. 3e).

To rule out potential carotid artery ligation-related perfusion fixation artifacts on measured Δ_fADC values, the Δ_fADC maps acquired from control, sham-operated, and HI-injured P8 mouse brains were compared (Fig. 4). The Δ_fADC measurements in sham-operated mice that underwent unilateral carotid artery ligation without hypoxia did not differ significantly

from those of control mice. In comparison, the regional damage to the ipsilateral CA1 Py layer in the HI-injured group could be clearly seen in the group-averaged Δ_fADC maps (Fig. 4a). Mean Δ_fADC values in the ipsilateral Py layer in HI-injured mice were significantly lower compared to the contralateral side ($p < 0.01$) and the control group ($p < 0.01$). Fig. 4b–c shows the mean ADC values in the ipsilateral and contralateral Py and GrDG regions from P8 mouse brains plotted against gradient oscillation frequency. In the pulsed-gradient diffusion measurements (denoted by 0 Hz in the plots in Fig. 4), no significant difference in ADC values between the ipsilateral and contralateral Py layers was observed in the HI-injured mice. However, significant ($p < 0.005$) differences were detected between the ipsilateral and contralateral Py regions in ADC values measured with oscillating gradient dMRI at increasing frequencies of 50, 100, and 150 Hz (Fig. 4b). The GrDG layer exhibited no significant differences in ADC measurements between the ipsilateral and contralateral sides 1 day after HI at any of the tested oscillation frequencies (Fig. 4c).

Spatiotemporal evolution of oscillating gradient dMRI contrasts in the hippocampus following neonatal HI

Oscillating gradient dMRI of mouse brains at 1, 4 and 8 days following HI revealed the regional and temporal evolution of neurodegeneration in the hippocampal layers, as evidenced by spatiotemporal changes in Δ_fADC contrasts. Fig. 5 shows the group-averaged Δ_fADC maps from control and HI-injured brains at P8, P11, and P15. At day 1 after exposure to HI (P8), the decrease in Δ_fADC values was confined to the Py layer in the ipsilateral hippocampus, with no marked difference observed in the dentate gyrus. Similar to the observations at day 1, the ipsilateral Py layer continued to exhibit significantly lower Δ_fADC values compared to control and contralateral measurements at 4 and 8 days post-injury. By day 8 (P15), the Py layer in the CA1 hippocampal region was barely discernible in the Δ_fADC maps (indicated by the white arrows in Fig. 5a). Compared to the Py layer, a noticeable decrease in Δ_fADC in the ipsilateral GrDG region was observed only later, at day 4 after the injury (P11). Quantitative measurements of Δ_fADC values at 1, 4 and 8 days following HI (Fig. 5b) revealed no significant differences in the GrDG region at day 1, while significant decrease in the ipsilateral measurements was observed at day 4 ($p < 0.01$) and day 8 ($p < 0.01$) relative to contralateral values. Compared to the Py layer, the decrease in Δ_fADC in the ipsilateral GrDG region was less severe at both P11 and P15, and was not observed in all mice subjected to HI. These observations suggested that while the Py layer showed regional neurodegeneration as early as on day 1 post-injury, damage to the GrDG region occurred at a relatively delayed interval and with variable severity after the initial insult.

H&E-stained histological sections through the hippocampus from representative HI-injured mouse brains at 4 and 8 days post-injury (at P11 and P15) are shown in Fig. 6, along with the corresponding Δ_fADC maps. H&E staining indicated continued neurodegeneration in the Py region at day 4 after the injury (Fig. 6c–d), and consistent with the MR-based findings, regional neuronal damage was also evident in the ipsilateral GrDG layer at this stage (Fig. 6i–j). By P15, the Py layer in the ipsilateral CA1 region exhibited extensive pyramidal cell loss and overall decreased neuronal density in the H&E-stained sections (Fig. 6e–f). Localized neuronal loss was also seen in the ipsilateral GrDG layer compared to the

contralateral side in the P15 brain (Fig. 6k–l), in regions that corresponded to the areas of reduced signal intensity observed in the Δ_fADC contrasts (shown in Fig. 6h). Fluoro-Jade C stained sections did not show active degenerating neurons at either of these stages (data not shown).

DISCUSSION

This study investigated the application of oscillating gradient dMRI to characterize neurodegeneration in the neonatal mouse hippocampus following HI. Our findings show that the technique could detect early morphological changes associated with neurodegeneration in the hippocampal Py and GrDG layers in the neonatal mouse brain. Comparisons with histopathological assessment showed that changes in the observed Δ_fADC contrasts corresponded closely with histologic evidence of neuronal injury in the studied regions. These results indicate that the frequency-dependence of ADC measurements using oscillating gradient dMRI can potentially allow us to quantitatively examine the degree and extent of neurodegeneration in the hippocampus after neonatal hypoxic ischemic injury.

There have been several studies using oscillating-gradient diffusion MRI to probe restricted diffusion in biological tissues [20, 27, 28, 30]. A few recent reports have also demonstrated the application of this technique to investigate structural changes associated with pathology in animal models. Does *et al.* reported increased ADC dependence on diffusion time in rat brains with global ischemia [27]. Colvin *et al*. showed increased ADC contrast between glioblastoma tumors and surrounding tissues using oscillating gradient dMRI at increasing frequencies in rats [29]. The rate of frequency-dependent increase of perpendicular diffusivity measurements with this technique was shown to be significantly elevated in the corpus callosum in a mouse model of cuprizone-induced demyelination [31]. Here, we showed that similar to previous findings in the adult mouse brain [31], the neonatal mouse brain exhibits unique tissue contrasts with increasing gradient frequencies, highlighting the hippocampal Py and GrDG layers as well as regions in the cerebellum, which are relatively difficult to delineate using standard relaxometry-based or pulsed-gradient diffusion MR contrasts. We found that the rate of frequency-dependent increase in ADC in the hippocampal layers shows a significant decrease in response to neonatal HI-injury, and the regions in which this decrease is detected correspond specifically with regions showing local neuronal degeneration on histologically-stained tissue sections. These findings show that the anatomical contrasts generated using high-resolution oscillating-gradient dMRI can provide a means to uniquely examine neuronal degeneration and grey matter injury in the mouse brain.

An interesting observation in the present study was that the rate of frequency-dependent increase in ADC in the CA1 Py layer of uninjured (control) mice showed a progressive decrease with age from P8 to P15 (the plot in Fig. 5b). Table 1 presents a comparison of the measured Δ_fADC values in the Py and GrDG layers from P8, P11, P15, and adult (P60) C57BL6 mouse brains, from ROIs at the level of the dorsal hippocampus at each age. Data used for measurements for the adult brains are obtained from our previous study [31]. At P8, the Py layer exhibited significantly higher Δ_fADC values compared to previous observations in the adult C57BL6 brain, and by P15 the mean Δ_fADC had decreased significantly (~61%

of values at P8, $p < 0.005$), approaching the values measured in adult brains. In comparison, the GrDG layer showed no significant age-related changes in Δ_fADC measurements. Quantitative data on the morphological changes occurring in neuronal layers of the hippocampus during early postnatal mouse brain development are limited. H&E staining of the CA1 Py layer at P8, P11, and P15 from control mouse brains in our study (Figure 7) shows a progressive increase in the pyramidal cell soma size with age. At P8, the pyramidal cells are very densely packed, with cell bodies stacked in multiple rows. The P15 brain shows fewer rows of pyramidal cells, along with an increase in the cell diameter and reduced cell packing density (Fig. 7a–c). These observations are similar to a previous electron microscopy study in the rabbit brain [40], that showed a remarkably high cellular density in the CA1 Py layer of immature animals, with increasing soma area and a steady decrease in cell packing density during early postnatal maturation. Although this was not a focus of the present study, exploring how the Δ_fADC contrasts in different brain regions evolve during brain development can potentially yield additional insights into the contrast mechanisms of this technique.

The Δ_fADC maps of control and HI-injured mouse brains imaged at 1, 4 and 8 days following HI revealed the regional and temporal evolution of neuronal injury in the hippocampus. We found early changes in Δ_fADC contrasts in the Py cell layer of the hippocampal CA1 region (at 24 hours post-HI), with relatively delayed onset of changes observed in the GrDG layer. HI has been previously shown to lead to selective cell death of CA1 pyramidal neurons and granule cells in the dentate gyrus in the neonatal mouse brain, at 24–72 hours following injury [9, 41, 42]. In our study, compared to the Py region, significant differences in Δ_fADC measurements between the ipsilateral and contralateral GrDG regions were first detected at day 4 after HI-injury. As seen in Figs. 3 and 6, regional changes in Δ_fADC contrasts in the Py and GrDG layers observed in HI-injured mice in each age-group were mirrored by regional neuropathology seen from histological assessment in the same animals (Figs. 3, 6). These findings suggest that regional differences in the progression of HI-induced neurodegeneration in the hippocampus could be sensitively detected by Δ_fADC contrasts. Further, we observed a higher reduction in Δ_fADC values in the Py layer compared to the GrDG layer (Fig. 5b), consistent with histologic evidence of less severe neuronal loss in the GrDG region seen with H&E staining. These observations are similar to a previous report using the Vanucci neonatal mouse model of HI, that showed delayed and less severe neurodegeneration of granule cells in the dentate gyrus compared to pyramidal cells in the CA1 region using Toluidine blue staining [7].

The range of gradient oscillation frequencies used in our study corresponds to effective diffusion times extending from 1.67 ms to 15 ms, equivalent to free water root-mean-square displacements of 3 μm to 9.2 μm at 37°C. Therefore, the changes in the rate of frequency-dependent increase in ADC measurements following HI reflect underlying changes in tissue microstructure occurring at spatial scales within this range. The areas of local pyramidal and granule cell loss seen with H&E staining suggest that the observed contrast changes in Δ_fADC maps potentially reflect alterations in the neuronal cell packing density in these regions. HI-induced neurodegeneration involves an array of complex biochemical and molecular mechanisms, that are accompanied by astrogliosis and microglial activation. Although the precise mechanisms of neuronal injury after HI have not been completely

elucidated, previous reports using electron microscopy have shown evidence of distinctive changes in pyramidal and granule cell morphology. For instance, degenerating pyramidal cells in the neonatal mouse hippocampus were shown to exhibit greatly condensed nuclei immediately after HI, with vacuolization of the cytoplasm [7]. Since the ratio of nuclear volume to cellular volume, or nuclear volume fraction, has been shown to influence the rate of ADC increase with gradient frequency in a previous simulation-based study [23], reduction in the cell nuclei size could also contribute to an observed decrease in Δ_fADC measurements. However, our current understanding of the relative contributions of intracellular and extracellular compartments to the frequency-dependent contrasts observed with oscillating gradient dMRI is not complete. Further morphological analyses of cellular populations in the Py and GrDG hippocampal layers following HI can potentially provide additional insights into other underlying neuropathological changes that contribute to the observed Δ_fADC decrease in this model.

One potential technical limitation of oscillating gradient dMRI experiments is the relatively high gradient strength needed to generate the desired tissue contrasts. The gradient strengths used in our study (e.g., 390 mT/m for a b-value of 700 s/mm^2 at 150 Hz) are well beyond the capability of gradient systems on existing clinical MRI scanners (~40 mT/m). The use of longer gradient waveforms (increasing the number of cycles) can potentially reduce the gradient strength requirement, but in turn poses a constraint on the achievable signal-to-noise ratio (SNR) due to the increased echo time. A few studies have recently demonstrated the feasibility of oscillating gradient dMRI on existing clinical scanners, by using specially designed gradient waveforms with lower b-values than those used in this study [43, 44]. It should also be noted that the data in our study were acquired from ex vivo fixed brain specimens. It is known that ADC measurements in tissues can be affected by postmortem processing and fixation procedures [45]. Therefore, quantitative comparison of absolute ADC values across subjects needs to be interpreted carefully. It has been shown that the use of higher b-values can potentially yield better contrasts in ex vivo tissue specimens [46], but the gradient strength requirement of oscillating diffusion-encoding waveforms limits the maximum attainable b-values for oscillating gradient dMRI on existing MRI scanners. In the future, combining faster acquisition modules such as echo planar imaging with oscillating diffusion-sensitizing gradients may reduce the acquisition times further to improve the feasibility of high-resolution 3D oscillating gradient dMRI of the in vivo mouse brain, which can enable longitudinal monitoring of HI-related hippocampal neurodegeneration using this technique.

In summary, this study demonstrated that oscillating gradient dMRI is uniquely sensitive to early neuronal degeneration in the neonatal mouse hippocampus following HI. The frequency-dependence of ADC contrasts with this method can be used to delineate areas of regional neuronal injury specifically in the Py and GrDG layers. These findings will be useful for investigations in neonatal HI mouse models, for quantitative evaluation of injury outcomes and therapeutic efficacy as well as to direct histopathological investigation towards specific regions of the hippocampus.

Acknowledgments

This study was supported by the National Institute of Health grants R01NS070909, R01HD074593, and R01HD070996.

References

1. Ferriero DM. Neonatal brain injury. N Engl J Med. 2004; 351(19):1985–95. [PubMed: 15525724]
2. Northington FJ. Brief update on animal models of hypoxic-ischemic encephalopathy and neonatal stroke. ILAR J. 2006; 47(1):32–8. [PubMed: 16391429]
3. Vannucci RC, Connor JR, Mauger DT, Palmer C, Smith MB, Towfighi J, Vannucci SJ. Rat model of perinatal hypoxic-ischemic brain damage. J Neurosci Res. 1999; 55(2):158–63. [PubMed: 9972818]
4. Northington FJ, Ferriero DM, Graham EM, Traystman RJ, Martin LJ. Early Neurodegeneration after Hypoxia-Ischemia in Neonatal Rat Is Necrosis while Delayed Neuronal Death Is Apoptosis. Neurobiol Dis. 2001; 8(2):207–19. [PubMed: 11300718]
5. Dijkhuizen RM, Knollema S, van der Worp HB, Ter Horst GJ, De Wildt DJ, van der Sprenkel JWB, Tulleken KAF, Nicolay K. Dynamics of cerebral tissue injury and perfusion after temporary hypoxia-ischemia in the rat - Evidence for region-specific sensitivity and delayed damage. Stroke. 1998; 29(3):695–704. [PubMed: 9506615]
6. Nakajima W, Ishida A, Lange MS, Gabrielson KL, Wilson MA, Martin LJ, Blue ME, Johnston MV. Apoptosis has a prolonged role in the neurodegeneration after hypoxic ischemia in the newborn rat. J Neurosci. 2000; 20(21):7994–8004. [PubMed: 11050120]
7. Sheldon RA, Hall JJ, Noble LJ, Ferriero DM. Delayed cell death in neonatal mouse hippocampus from hypoxia-ischemia is neither apoptotic nor necrotic. Neurosci Lett. 2001; 304(3):165–8. [PubMed: 11343828]
8. Liu CL, Siesjo BK, Hu BR. Pathogenesis of hippocampal neuronal death after hypoxia-ischemia changes during brain development. Neuroscience. 2004; 127(1):113–23. [PubMed: 15219674]
9. Miles DK, Kernie SG. Hypoxic-ischemic brain injury activates early hippocampal stem/progenitor cells to replace vulnerable neuroblasts. Hippocampus. 2008; 18(8):793–806. [PubMed: 18446826]
10. Qiu L, Zhu C, Wang X, Xu F, Eriksson PS, Nilsson M, Cooper-Kuhn CM, Kuhn HG, Blomgren K. Less neurogenesis and inflammation in the immature than in the juvenile brain after cerebral hypoxia-ischemia. J Cereb Blood Flow Metab. 2007; 27(4):785–94. [PubMed: 16926844]
11. Kuan CY, Schloemer AJ, Lu A, Burns KA, Weng WL, Williams MT, Strauss KI, Vorhees CV, Flavell RA, Davis RJ, Sharp FR, Rakic P. Hypoxia-ischemia induces DNA synthesis without cell proliferation in dying neurons in adult rodent brain. J Neurosci. 2004; 24(47):10763–72. [PubMed: 15564594]
12. Ment LR, Bada HS, Barnes P, Grant PE, Hirtz D, Papile LA, Pinto-Martin J, Rivkin M, Slovis TL. Practice parameter: neuroimaging of the neonate: report of the Quality Standards Subcommittee of the American Academy of Neurology and the Practice Committee of the Child Neurology Society. Neurology. 2002; 58(12):1726–38. [PubMed: 12084869]
13. Wendland MF, Faustino J, West T, Manabat C, Holtzman DM, Vexler ZS. Early diffusion-weighted MRI as a predictor of caspase-3 activation after hypoxic-ischemic insult in neonatal rodents. Stroke. 2008; 39(6):1862–8. [PubMed: 18420950]
14. Aden U, Dahlberg V, Fredholm BB, Lai LJ, Chen Z, Bjelke B. MRI evaluation and functional assessment of brain injury after hypoxic ischemia in neonatal mice. Stroke. 2002; 33(5):1405–10. [PubMed: 11988622]
15. Ten VS, Wu EX, Tang H, Bradley-Moore M, Fedarau MV, Ratner VI, Stark RI, Gingrich JA, Pinsky DJ. Late measures of brain injury after neonatal hypoxia-ischemia in mice. Stroke. 2004; 35(9):2183–8. [PubMed: 15272130]
16. Stone BS, Zhang J, Mack DW, Mori S, Martin LJ, Northington FJ. Delayed neural network degeneration after neonatal hypoxia-ischemia. Ann Neurol. 2008; 64(5):535–46. [PubMed: 19067347]

17. Wang S, Wu EX, Tam CN, Lau HF, Cheung PT, Khong PL. Characterization of white matter injury in a hypoxic-ischemic neonatal rat model by diffusion tensor MRI. Stroke. 2008; 39(8): 2348–53. [PubMed: 18535275]
18. Anderova M, Vorisek I, Pivonkova H, Benesova J, Vargova L, Cicanic M, Chvatal A, Sykova E. Cell death/proliferation and alterations in glial morphology contribute to changes in diffusivity in the rat hippocampus after hypoxia-ischemia. J Cereb Blood Flow Metab. 2011; 31(3):894–907. [PubMed: 20877389]
19. Lodygensky GA, West T, Moravec MD, Back SA, Dikranian K, Holtzman DM, Neil JJ. Diffusion characteristics associated with neuronal injury and glial activation following hypoxia-ischemia in the immature brain. Magn Reson Med. 2011; 66(3):839–45. [PubMed: 21394776]
20. Gore JC, Xu J, Colvin DC, Yankeelov TE, Parsons EC, Does MD. Characterization of tissue structure at varying length scales using temporal diffusion spectroscopy. NMR Biomed. 2010; 23(7):745–56. [PubMed: 20677208]
21. Schachter M, Does MD, Anderson AW, Gore JC. Measurements of restricted diffusion using an oscillating gradient spin-echo sequence. J Magn Reson. 2000; 147(2):232–7. [PubMed: 11097814]
22. Stepisnik J. Analysis of NMR self-diffusion measurements by a density matrix calculation. Physica B. 1981; 104:350–364.
23. Xu J, Does MD, Gore JC. Sensitivity of MR diffusion measurements to variations in intracellular structure: effects of nuclear size. Magn Reson Med. 2009; 61(4):828–33. [PubMed: 19205020]
24. Parsons EC Jr, Does MD, Gore JC. Temporal diffusion spectroscopy: theory and implementation in restricted systems using oscillating gradients. Magn Reson Med. 2006; 55(1):75–84. [PubMed: 16342147]
25. Stepisnik J, Lasic S, Mohoric A, Sersa I, Sepe A. Spectral characterization of diffusion in porous media by the modulated gradient spin echo with CPMG sequence. J Magn Reson. 2006; 182(2): 195–9. [PubMed: 16844392]
26. Parsons EC, Does MD, Gore JC. Modified oscillating gradient pulses for direct sampling of the diffusion spectrum suitable for imaging sequences. Magn Reson Imaging. 2003; 21(3–4):279–85. [PubMed: 12850719]
27. Does MD, Parsons EC, Gore JC. Oscillating gradient measurements of water diffusion in normal and globally ischemic rat brain. Magn Reson Med. 2003; 49(2):206–15. [PubMed: 12541239]
28. Colvin DC, Loveless ME, Does MD, Yue Z, Yankeelov TE, Gore JC. Earlier detection of tumor treatment response using magnetic resonance diffusion imaging with oscillating gradients. Magn Reson Imaging. 2011; 29(3):315–23. [PubMed: 21190804]
29. Colvin DC, Yankeelov TE, Does MD, Yue Z, Quarles C, Gore JC. New insights into tumor microstructure using temporal diffusion spectroscopy. Cancer Res. 2008; 68(14):5941–7. [PubMed: 18632649]
30. Portnoy S, Flint JJ, Blackband SJ, Stanisz GJ. Oscillating and pulsed gradient diffusion magnetic resonance microscopy over an extended b-value range: Implications for the characterization of tissue microstructure. Magn Reson Med. 2012; 69(4):1131–45. [PubMed: 22576352]
31. Aggarwal M, Jones MV, Calabresi PA, Mori S, Zhang J. Probing mouse brain microstructure using oscillating gradient diffusion MRI. Magnetic Resonance in Medicine. 2012; 67(1):98–109. [PubMed: 21590726]
32. Rice JE 3rd, Vannucci RC, Brierley JB. The influence of immaturity on hypoxic-ischemic brain damage in the rat. Ann Neurol. 1981; 9(2):131–41. [PubMed: 7235629]
33. Ditelberg JS, Sheldon RA, Epstein CJ, Ferriero DM. Brain injury after perinatal hypoxia-ischemia is exacerbated in copper/zinc superoxide dismutase transgenic mice. Pediatr Res. 1996; 39(2):204–8. [PubMed: 8825788]
34. Aggarwal M, Mori S, Shimogori T, Blackshaw S, Zhang J. Three-dimensional diffusion tensor microimaging for anatomical characterization of the mouse brain. Magn Reson Med. 2010; 64(1): 249–61. [PubMed: 20577980]
35. Conturo TE, McKinstry RC, Akbudak E, Robinson BH. Encoding of anisotropic diffusion with tetrahedral gradients: a general mathematical diffusion formalism and experimental results. Magn Reson Med. 1996; 35(3):399–412. [PubMed: 8699953]

36. Chuang N, Mori S, Yamamoto A, Jiang H, Ye X, Xu X, Richards LJ, Nathans J, Miller MI, Toga AW, Sidman RL, Zhang J. An MRI-based atlas and database of the developing mouse brain. Neuroimage. 2011; 54(1):80–9. [PubMed: 20656042]
37. Woods RP, Grafton ST, Holmes CJ, Cherry SR, Mazziotta JC. Automated image registration: I. General methods and intrasubject, intramodality validation. J Comput Assist Tomogr. 1998; 22(1): 139–52. [PubMed: 9448779]
38. Miller MI, Trouve A, Younes L. On the metrics and Euler-Lagrange equations of computational anatomy. Annu Rev Biomed Eng. 2002; 4:375–405. [PubMed: 12117763]
39. Schmued LC, Stowers CC, Scallet AC, Xu L. Fluoro-Jade C results in ultra high resolution and contrast labeling of degenerating neurons. Brain Res. 2005; 1035(1):24–31. [PubMed: 15713273]
40. Schwartzkroin PA, Kunkel DD, Mathers LH. Development of rabbit hippocampus: anatomy. Brain Res. 1981; 254(4):453–68. [PubMed: 7306827]
41. Fukuda T, Wang H, Nakanishi H, Yamamoto K, Kosaka T. Novel non-apoptotic morphological changes in neurons of the mouse hippocampus following transient hypoxic-ischemia. Neurosci Res. 1999; 33(1):49–55. [PubMed: 10096471]
42. Cho KO, Lee KE, Youn DY, Jeong KH, Kim JY, Yoon HH, Lee JH, Kim SY. Decreased vulnerability of hippocampal neurons after neonatal hypoxia-ischemia in bis-deficient mice. Glia. 2012; 60(12):1915–29. [PubMed: 22907804]
43. McHugh, DJ.; Hubbard, PL.; Zhao, S.; Parker, GJ.; Naish, JH. Distinguishing restricted diffusion and flow using pulsed and oscillating diffusion gradients at 1.5T. Proceedings of International Society for Magnetic Resonance in Medicine 20th Annual Meeting; 2012. p. 4109
44. Van AT, Holdsworth SJ, Bammer R. In vivo investigation of restricted diffusion in the human brain with optimized oscillating diffusion gradient encoding. Magn Reson Med. 201310.1002/mrm.24632
45. Shepherd TM, Thelwall PE, Stanisz GJ, Blackband SJ. Aldehyde fixative solutions alter the water relaxation and diffusion properties of nervous tissue. Magn Reson Med. 2009; 62(1):26–34. [PubMed: 19353660]
46. Sun SW, Neil JJ, Liang HF, He YY, Schmidt RE, Hsu CY, Song SK. Formalin fixation alters water diffusion coefficient magnitude but not anisotropy in infarcted brain. Magn Reson Med. 2005; 53(6):1447–51. [PubMed: 15906292]

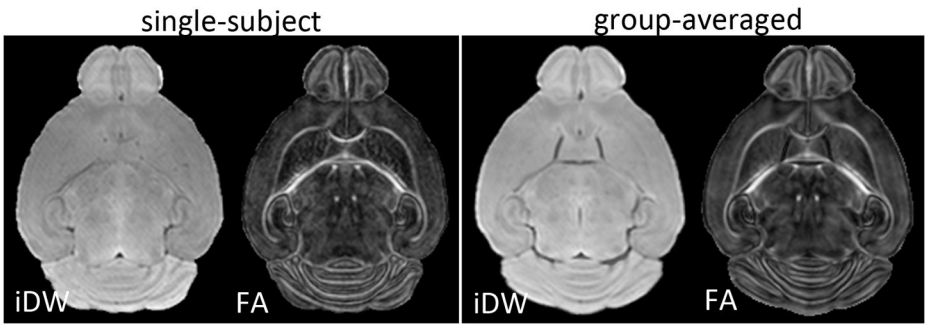

Figure 1.

Axial isotropic diffusion-weighted (iDW) and fractional anisotropy (FA) images from one representative mouse brain (left panel) and the group-averaged (n=5) iDW and FA images (right panel), from control mice at P11. The group-averaged images were generated using dual-channel large deformation diffeomorphic metric mapping driven by both iDW and FA contrasts.

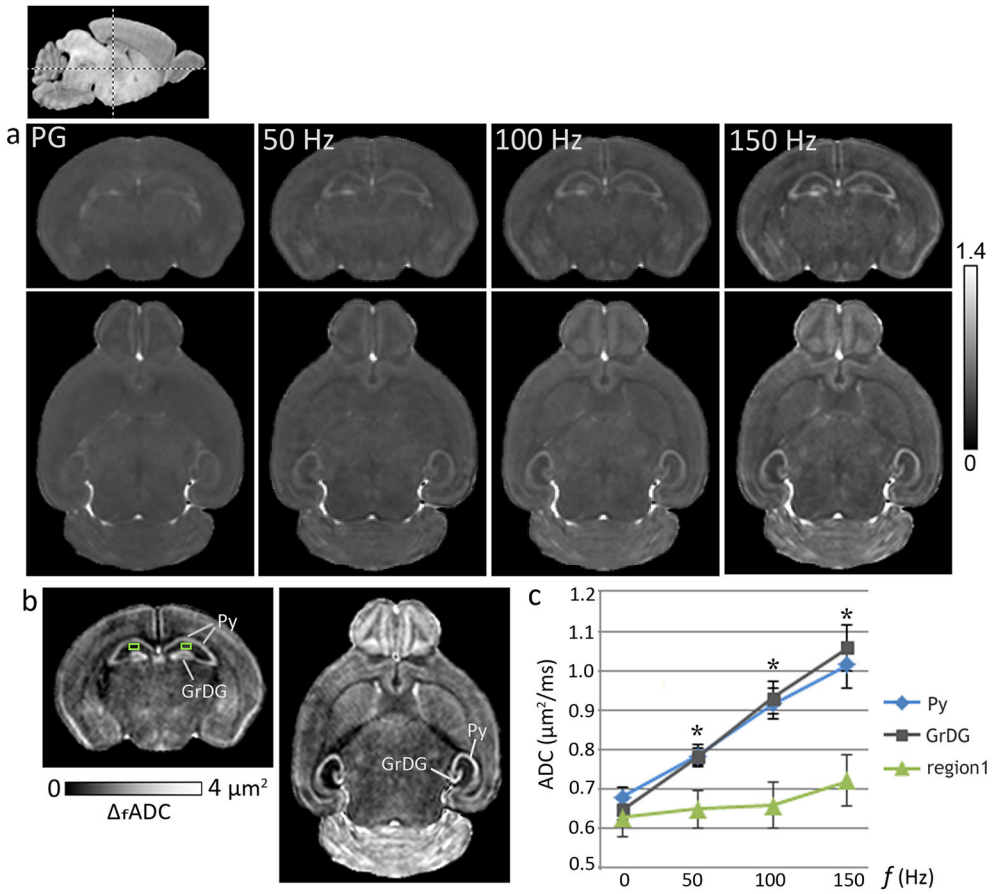

Figure 2.

Oscillating-gradient diffusion MRI revealed region-specific contrast enhancement in the neonatal mouse brain. a) ADC maps of a coronal (top panel) and an axial (bottom panel) section at the level of the hippocampus from a P8 brain, derived with pulsed-gradient (PG) and oscillating-gradient (50, 100, and 150 Hz) diffusion-weighted sequences are shown. The anatomic locations of the sections are indicated in the scout sagittal image at the top left. The units of ADC shown are $\mu m^2/ms$. b) Maps derived from a linear fitting of the ADC measurements with gradient frequency (Δ_fADC) revealed anatomical contrasts highlighting the pyramidal cell layer in the hippocampus (Py) and the granular cell layer in the dentate gyrus (GrDG). c) Plot of ADC measurements versus gradient frequency shows the significantly higher frequency-dependent ADC increase observed in the Py and the GrDG layers compared to adjacent hippocampal regions, e.g., a region in the CA1 subfield (region 1, indicated by the green squares in (b)). Averaged ADC measurements from both left and right hippocampal layers from P8 control mice are shown, with the pulsed-gradient measurements denoted by 0 Hz. *indicates significant ($p < 0.005$) differences in ADC values in both Py and GrDG layers compared to region 1. Error bars indicate standard deviations (n=5).

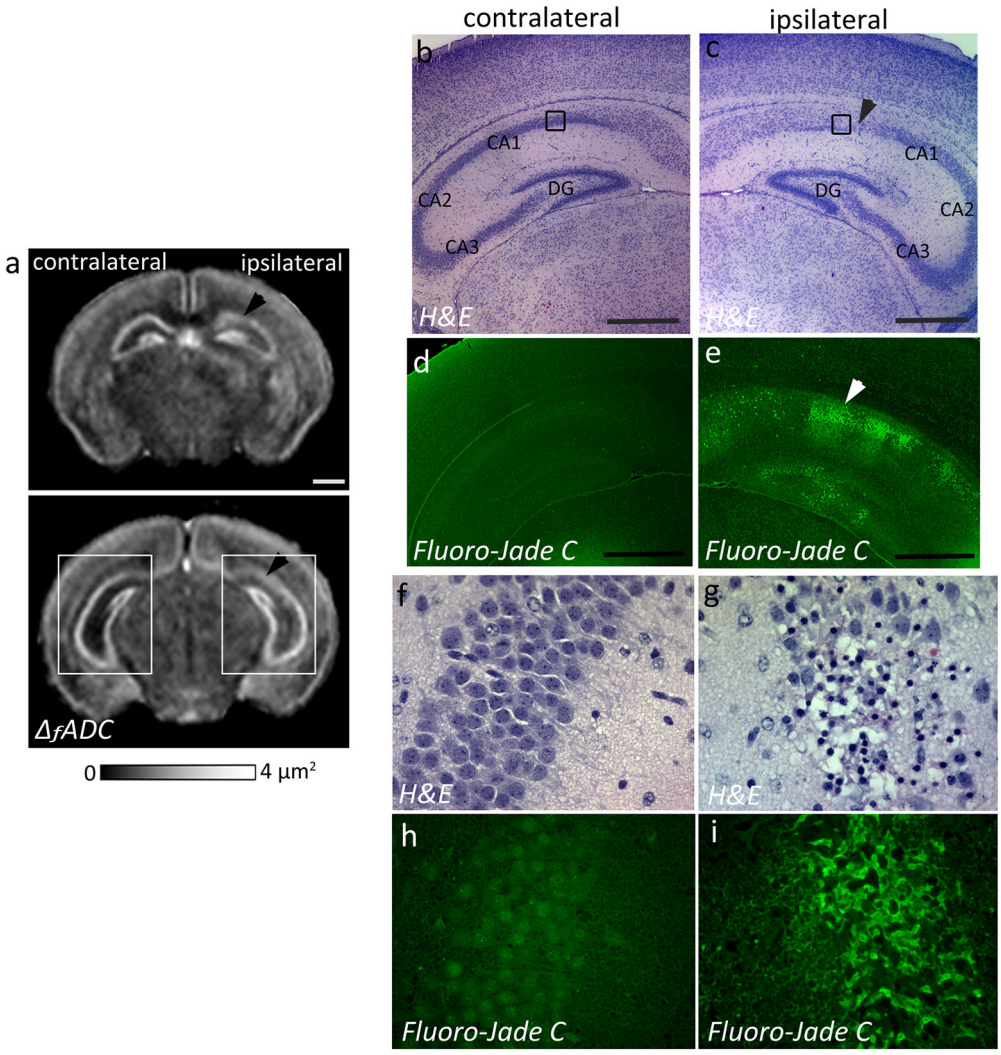

Figure 3.

Oscillating-gradient diffusion MRI and histopathological assessment of hippocampal injury at twenty-four hours after neonatal HI (at P8). a) Coronal sections at the level of the hippocampus from a P8 brain show regional decrease in Δ_fADC measurements in the pyramidal cell layer of the ipsilateral injured hippocampus (black arrowheads), compared to the contralateral side. b–c) H&E-stained sections within the areas indicated by the white squares in (a) (sections in (b–c) are rotated by 45° with respect to the Δ_fADC map in (a)) reveal interrupted staining of neuronal cell bodies in the ipsilateral CA1 Py layer, in areas corresponding to the regions of decreased intensity in the Δ_fADC map (black arrowhead). d–e) Fluoro-Jade C labeled sections reveal fluorescent signal located primarily in the Py layer of the ipsilateral hippocampus, with scattered Fluoro-Jade staining in the dentate gyrus at this stage. f–g) High-magnification views of the H&E-stained sections within the area indicated by black squares in (b,c) show neuronal injury and damage in the ipsilateral Py layer, with no evident damage to the contralateral region. h–i) High-magnification views of Fluoro-jade C labeled sections show degenerative changes in the ipsilateral Py layer. Scale bars = 0.5 mm.

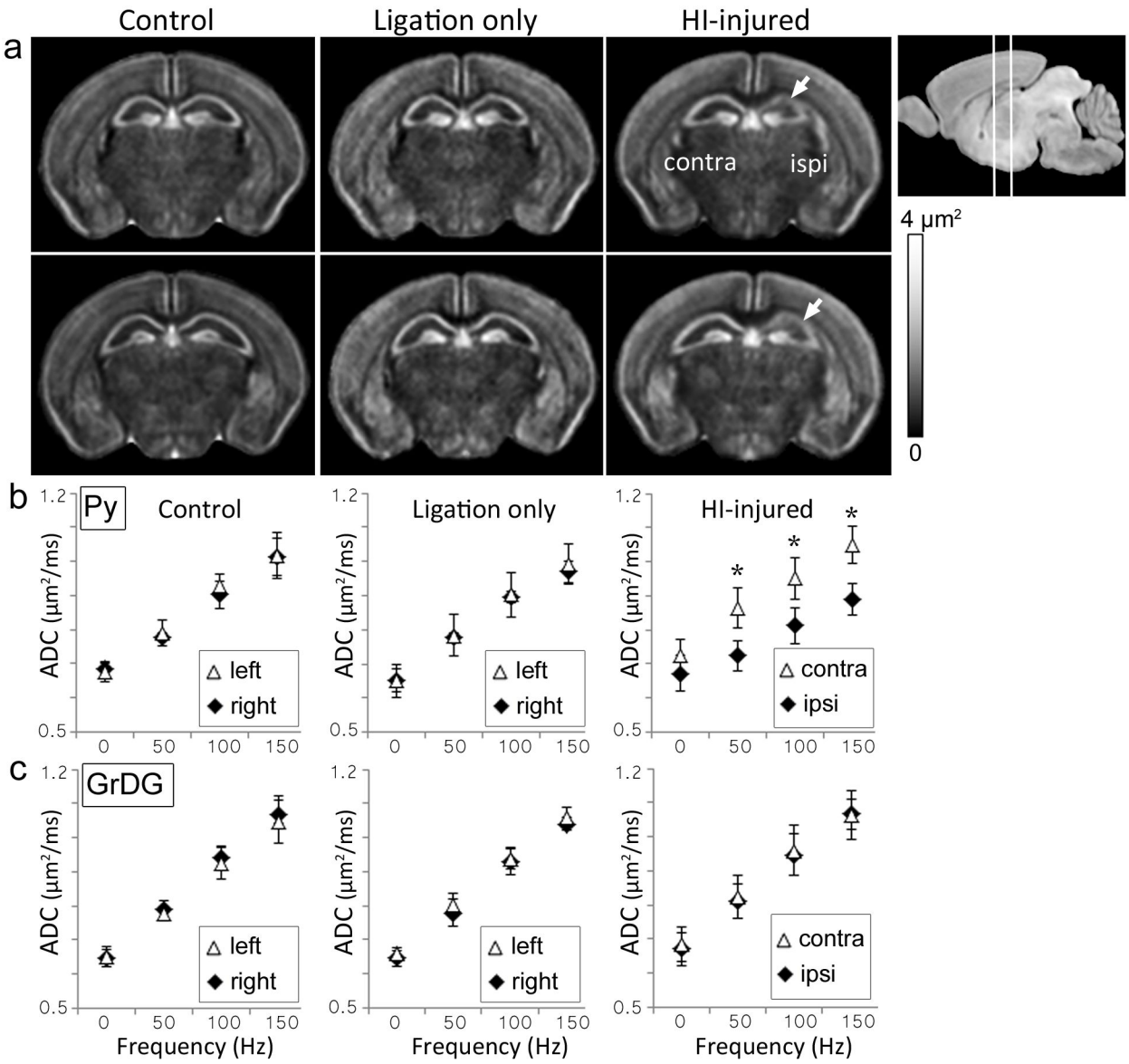

Figure 4.

Oscillating-gradient diffusion MRI of control, sham-operated (unilateral carotid artery ligation only), and HI-injured mouse brains at P8. a) Group-averaged Δ_fADC maps of control (n=5), ligation-only (n=3), and HI-injured (n=5) mouse brains show two coronal sections at the level of the hippocampus. The anatomical locations of the sections are shown in the scout image at the top right. White arrows indicate regional decrease in Δ_fADC measurements in the ipsilateral hippocampus observed in the HI-injured group. b–c) Plots of ADC values (mean ± standard deviation) versus gradient frequency for the Py and GrDG regions for the three cohorts. Mean ADC measurements from symmetric regions-of-interest in the left and right hippocampal layers are shown. Error bars represent standard deviations across subjects for each group. *indicates significant ($p<0.005$) differences in ADC measurements between the contralateral and ipsilateral regions.

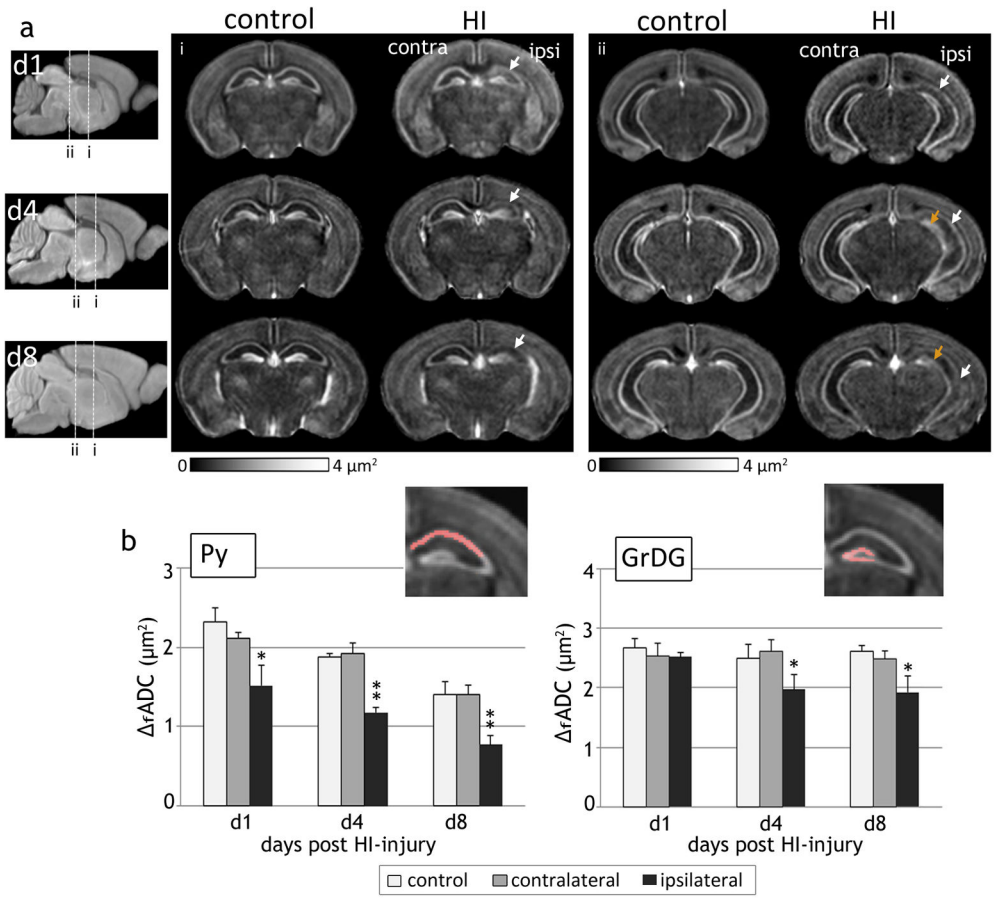

Figure 5.

Spatiotemporal evolution of Δ_fADC contrasts in the mouse hippocampus after exposure to neonatal HI at P7. a) Group-averaged Δ_fADC maps of control and HI-injured mouse brains at 1, 4, and 8 days following injury (at P8, P11 and P15, n=5 per group at each time point) show the regional and temporal progression of injury in the ipsilateral Py (white arrows) and GrDG (orange arrows) regions. Two coronal sections at the level of the hippocampus at each age are shown. The anatomical locations of the sections are indicated in the group-averaged iDW scout images at each age. b) Quantitative measurements of Δ_fADC values (mean ± standard deviation, n=5) in the Py and GrDG regions from control and HI-injured groups at 1, 4 and 8 days following HI. Values shown are measured from symmetric regions-of-interest in the contralateral and ipsilateral hippocampal regions (shown in the inset images). *p<0.01 and **p<0.005 compared with measurements from the contralateral hippocampus.

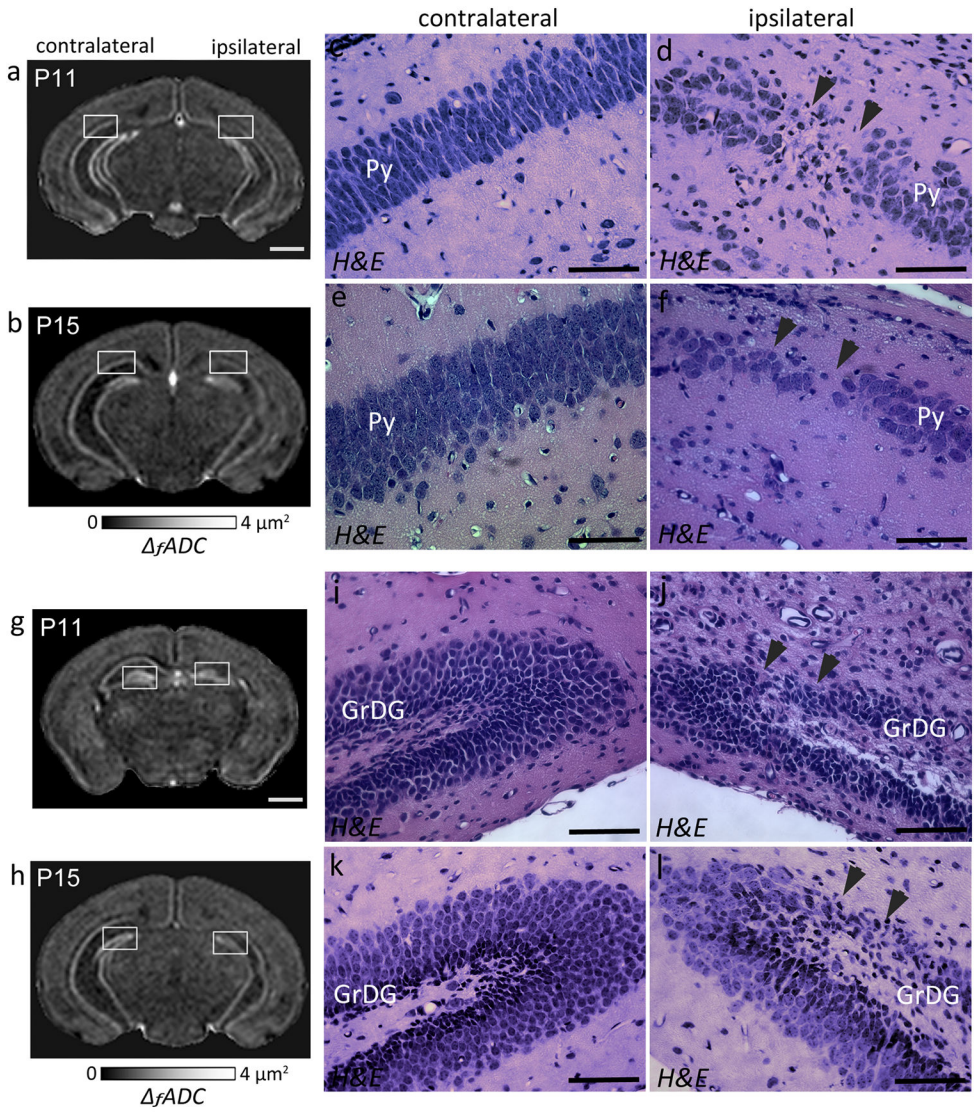

Figure 6.

Δ_fADC contrasts and histological evaluation showing regional neurodegeneration in the ipsilateral hippocampal layers at 4 (P11) and 8 (P15) days post exposure to HI-injury. a–b) Coronal sections through a P11 (a) and a P15 (b) mouse brain show regional decrease in Δ_fADC in the ipsilateral Py layer compared to the contralateral side. c–f) High-magnification views of H&E-staining through the hippocampi of the same mice (corresponding to the areas within the white squares in a and b, respectively). The H&E-stained sections show regional neuronal loss and reduced cell density in the ipsilateral Py layer (black arrowheads) compared to the contralateral region at 4 (c,d) and 8 (e,f) days after the injury. g–h) Coronal sections showing regional decrease in Δ_fADC in the ipsilateral GrDG layer, at P11 (g) and P15 (h). i–l) High-magnification views of H&E-stained sections corresponding to the white squares in g and h show regional neuronal loss in the GrDG layer of the ipsilateral hippocampus (black arrowheads). Scale bars for the MR images = 1 mm. Scale bars for the histology sections = 200 μm.

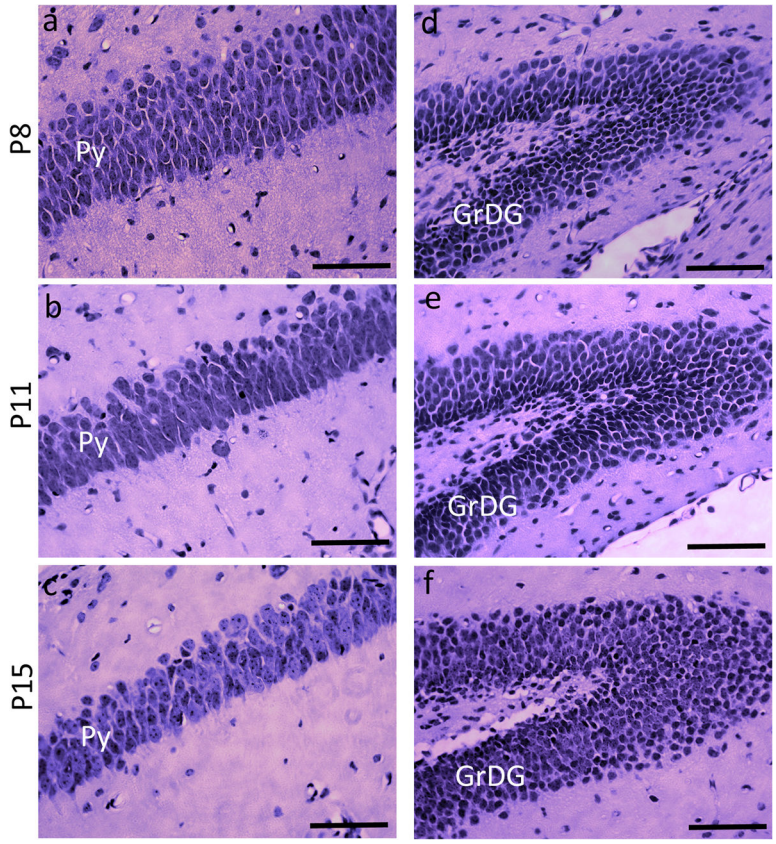

Figure 7.

H&E-stained sections showing the pyramidal cell layer (Py) and the granule cell layer of the dentate gyrus (GrDG), taken from control mice at P8, P11, and P15. a–c are sections through the Py layer, and d–f are sections through the GrDG layer from the left hippocampus at each age. Scale bars = 200 μm.

Table 1

Δ_fADC measurements in the CA1 pyramidal layer (Py) and the granule cell layer in the dentate gyrus (GrDG) from control C57BL6 mouse brains at different ages. Measurements are from ROIs at the level of the dorsal hippocampus (as indicated in Fig. 5) at each age.

Age	Δ_fADC in the Py layer (μm^2)	Δ_fADC in the GrDG layer (μm^2)
P8	2.33 ± 0.19	2.68 ± 0.12
P11	1.87 ± 0.04	2.50 ± 0.17
P15	1.40 ± 0.13	2.55 ± 0.09
P60	1.37 ± 0.04	2.52 ± 0.10

Data are shown as mean ± standard deviation (n=5 at each age). The P60 measurements are from adult mouse data from our previous study [31].